Applied Surface Science 436 (2018) 1–10

Contents lists available at ScienceDirect

Applied Surface Science

journal homepage: www.elsevier.com/locate/apsusc

Full Length Article

# Effect of copper coating on fibers made of aluminum alloy, titanium, and FeCrAl alloy on surface morphology and activity in CO oxidation

I.V. Lukiyanchuk[a], V.S. Rudnev[a,b,*], M.M. Serov[c], B.L. Krit[c], G.D. Lukiyanchuk[d], P.M. Nedozorov[a]

[a] Institute of Chemistry, Far Eastern Branch, Russian Academy of Sciences, Vladivostok, Russia
[b] Far Eastern Federal University, Vladivostok, Russia
[c] Moscow Aviation Institute (National Research University), Moscow, Russia
[d] PJSC Dal'pribor, Vladivostok, Russia

ARTICLE INFO

*Article history:*
Received 18 July 2017
Received in revised form
27 November 2017
Accepted 30 November 2017
Available online 5 December 2017

*Keywords:*
Metal fibers
Rapid solidification
Copper deposition
CO oxidation
Surface morphology

ABSTRACT

The catalytic activity of both copper fibers and copper-coated fibers of a diameter of 50–100 μm made of aluminum alloy, technical grade titanium, and FeCrAl alloy in CO oxidation has been estimated. Metal fibers have been fabricated by the method of pendant drop melt extraction (PDME). The fibers copper plating was carried out by chemical and electrochemical methods. The composition and structure of samples and coatings before and after catalytic tests have been characterized by the methods of scanning electron microscopy, energy-dispersive analysis, and X-ray fluorescence analysis. It has been shown that the catalytic activity of copper-coated fibers made of FeCrAl alloy in the reaction of CO oxidation is not inferior to that of copper fibers.



## 1. Introduction

Investigation of properties and fields of application of metal catalysts, carriers and catalytic filters in the form of honeycomb structures prepared from foil [1,2], wire gauzes [3–5], including woven and knitted ones [6,7], and nonwoven fibrous materials [8,9] is of interest due to their practically important properties. The design of a catalyst in the form of fibers in the composition of metallic wool or non-woven materials characterized with large geometric surface area and low hydrodynamic resistance to the flow of gases or liquids enables one to conduct processes within short contact times, thus achieving a complete reagent transformation. Moreover, such catalysts are characterized with high electrical and thermal conductivity, and the fibers themselves can be packaged in different ways. These properties create advantages for fibrous catalysts as compared to traditional monolithic, granular, or powdered ones.

One of the advanced and technologically reliable ways of fabrication of inorganic fibers and porous materials from them is the method of rapid solidification via melt spinning and its variant – the pendant drop melt extraction (PDME) method [10,11]. In the PDME method, fine fibers of stable sizes can be produced through precise controlling of the material feed to the melting zone and the adhesion interaction of the melt and the disk. The PDME method enables one to form elongated fibers of an equivalent diameter of 30–80 μm, individual particles of a length of 3–10 mm, as well as porous nonwoven sheet materials [11]. One of the advantages of the PDME method consists in application of crucibleless melting, which allows fabricating the fibers made from refractory and chemically active metals, including nickel, copper, titanium, zirconium, and heat-, corrosion-, and deformation-resistant steels and alloys [10–14]. Forming the fiber from the melt by means of the PDME method occurs at cooling rates of up to $10^6$ K/s, which results in formation of a metastable structure and emergence of solidification structures on the fiber surface. Due to the above, the fibers have high chemical activity and an increased concentration of defects and dopants on their surface, which is favorable for applications in catalysis.

The application of the method of rapid solidification results in an increase in the catalytic activity of the fabricated materials as compared to that of the initial bulk alloys, which was shown in [8,9,15–18] for hydrogenation of nitrobenzene, dinitrotoluenes, adiponitrile, and isophorone on Ni-based alloys [8,9,15,16] and for Fischer-Tropsch synthesis on skeletal Fe-based catalysts [17,18].

* Corresponding author at: Institute of Chemistry, Far Eastern Branch, Russian Academy of Sciences, Vladivostok, Russia.
*E-mail address:* rudnevvs@ich.dvo.ru (V.S. Rudnev).

https://doi.org/10.1016/j.apsusc.2017.11.287
0169-4332/

The catalytic activity of the fibers fabricated by the PDME method in CO oxidation was studied in [19]. It has been demonstrated that in the model reaction of CO oxidation copper fibers are the most active among the studied metal fibers. The activity of the studied fibrous samples decreases in the series: Cu > Ni-Cu-Mn-Si > Ni-Cr-Al-Pt-Ir-Hf ~ Ni-Cr-Al-Pt-Hf > Ni-Cr-Ti-W-Mo-Nb ≈ Ni-Cr-Al-REM > Fe-Cr-Al-needles > Ni-Cr-Al-Mo-Hf > Fe-Cr-Al fibers ≥ Fe-Cr-Al-Pt > Al-Mg-Cu > Ti. High activity of copper fibrous catalysts can be associated with the formation of copper oxides on their surfaces [20]. It is worth mentioning that copper fibers are not only more active in CO oxidation, but also cheaper than those containing up to 10 wt.% of platinum group metals [19].

Copper-based catalysts have attracted much attention in heterogeneous catalysis [20–33] and photocatalysis [34–37] due to their low cost and high selectivity and high catalytic activity in many catalytically important processes. Copper and its compounds are contained in many advanced industrial catalysts [38,39]. Cu-based catalysts are characterized with high activity in deep oxidation of carbon monoxide [20–27] and hydrocarbons [24,27], preferential oxidation of CO in $H_2$-rich stream [28], water–gas shift reaction [29,30], selective reduction reactions [31,32], and methanol reforming [33]. It has been found that the activity of the $CuCr_2O_4$ spinel in CO oxidation is comparable to that of Pd and Pt [25,40], but at the same time this material is superior to Pt- and Pd-based catalysts due to its high thermal stability and exceptional chemical resistance to impurities, such as sulfur compounds [21,23]. Unlike noble metal catalysts that are expensive and poisoned by nitrogen and sulfur oxides, the advantage of these copper-based catalysts consists in the fact that they are cheap, mechanically strong, and relatively stable to contaminants [26].

Even without any pretreatment, copper foil has a certain activity in the oxidation of CO and $CH_4$ [24]. Specially treated copper microchannel plates serve as a basis for creating microreactors for catalytic gas-phase oxidation [41,42]. In some cases, copper is subject to special treatment yielding the growth of nanosized copper oxides in the form of rods, sheets, flowers, whiskers, etc. on its surface, thus increasing the specific surface area and activity of Cu-based catalysts [34–37,41,43]. At the same time, the use of bulk Cu-containing alloys is not always justified in terms of comparatively high density and cost and insufficient heat resistance of copper. Therefore, it is of interest to investigate the behavior of copper layers deposited on metallic fibers of different nature, taking into account the possible effect of the fiber composition on the catalytic properties of the resulting compositions.

The objective of the present work was to perform a comparative analysis of the composition, surface morphology, and activity in CO oxidation of copper layers deposited on the fibers made of aluminum alloy, titanium and FeCrAl alloy by chemical and electrochemical methods.

## 2. Experimental

### 2.1. Fabricating the metal fibers

M.M. Serov fabricated metal fibers at the Chair of Technologies of Automated Design of Metallurgical Production of the Moscow Aviation Institute.

Fig. 1 schematically shows the operation principle of an apparatus for producing metal fibers and non-woven materials by the PDME technique [12].

The main feature of the PDME method consists in the fact that the molten metal in a free state forms a drop overhanging from the lower butt end of a vertical rod. The drop contacts with the top of the trigonal leading edge of the cooled rotating heat receiver. In the contact zone, the melt solidifies. The heat receiver rotation results in the removal of the material from the melt and its dispersal to the collector by centrifugal forces.

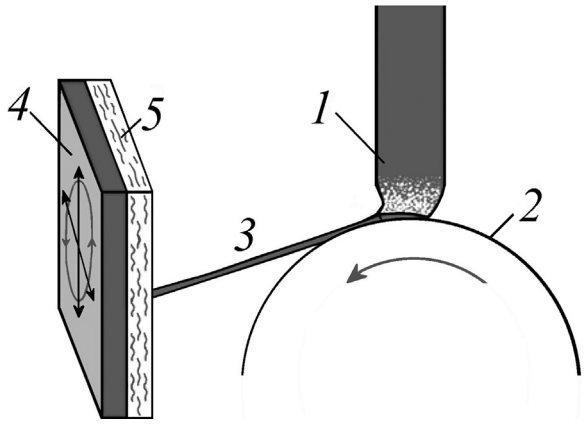


**Fig. 1.** Schematic diagram of forming porous fibrous materials by the PDME method: (*1*) dispersing billet, (*2*) rotating heat receiver, (*3*) metal fiber, (*4*) movable (receiving) surface, (*5*) porous material formed from fibers.

To fabricate fibers, we used copper (M2 grade), titanium (VT1-0 grade), aluminum alloy of the Al-Mg-Cu system, and FeCrAl alloy.

### 2.2. Copper deposition on metal fibers

Copper coatings were obtained by electroplating and electroless plating at room temperature (Fig. 2).

Electroless copper plating was used only for aluminum alloy fibers (Fig. 2b). Preliminarily, the fibrous samples were degreased for 1 min in ethanol, washed with warm running water, etched for 1 min in solution of 100 g/L NaOH, and rinsed with warm running water once again. The copper plating was carried out for 2 min in an aqueous solution containing 20 g/L $CuSO_4 \cdot 5H_2O$, 35 g/L glycerol, 26 g/L NaOH and 8 mL/L of 40% formaldehyde solution as reducing agent [44].

Copper electroplating was used for fibers made of titanium and FeCrAl alloy, Fig. 2c. Preliminarily, the fibrous samples were degreased with ethanol for 1 min, washed with warm running water, and etched in a mixture of concentrated acids containing 60 g/L of concentrated nitric acid and 60 g/L of concentrated hydrofluoric acid. Electroplating was carried out in the copper sulfate electrolyte (230 g/L of $CuSO_4 \cdot 5H_2O$, 60 g/L of concentrated sulfuric acid and 8 g/L of ethanol) according to Russian State Standard (GOST) 107.460092.001-86. The electrochemical cell consisted of a thermal glass of 1.0 L in volume with two anodes made of 0.5 mm thick copper foil, which were located in opposite to each other. The cathode made of metal fibers was placed between two anodes in the center of the electrochemical cell. Each of the anodes had a surface area of 50 $cm^2$ and the geometrical area of the fibers was about 100 $cm^2$. A matrix MPS-3010L-1 laboratory power supply unit (Russia) was used. The processing time was 2 min, and the cathode current density was 0.05 A/$cm^2$. Such a current density was selected experimentally, since burning of the fibers was observed with higher current density.

In both cases, upon copper plating, copper-coated metal fibers were again washed with warm running water and dried with compressed air.

Hereinafter, for simplicity, copper-coated fibers will be denoted as Cu/Ti, Cu/Al, and Cu/FeCrAl.

### 2.3. Characterization of initial and copper-coated fibers

The composition and structure of the samples and coatings were characterized by the methods of scanning electron microscopy

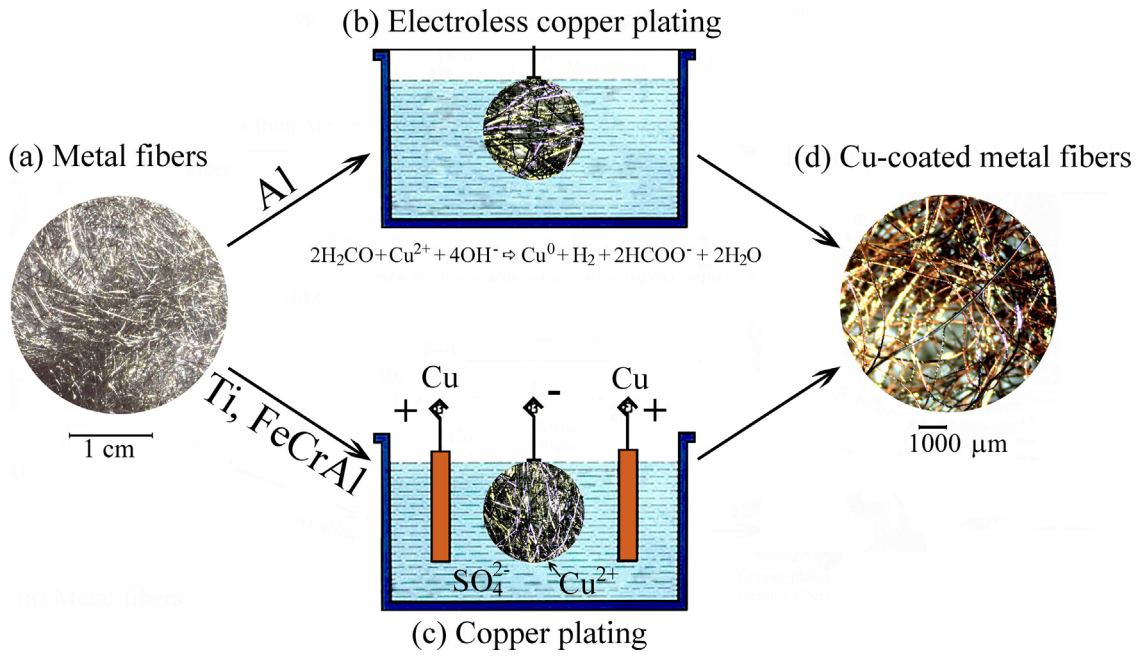


**Fig. 2.** The scheme of fabrication of copper-coated fibers by electroless copper plating (b) and copper plating (c), appearances of initial metal fibers (a) and copper-coated metal fibers (d).

(SEM), X-ray fluorescence (XRF) analysis, energy dispersive X-ray spectroscopy (EDS), and X-ray microprobe analysis.

The initial fibers composition was determined using an X-MET 7500 X-ray fluorescence portable analyzer (Oxford Instruments, United Kingdom). The depth of penetration of the scanning beam was ~10–20 μm.

The data on the samples' surface morphology and element composition of the fibers made of copper, titanium, and aluminum alloy in the Al-Mg-Cu system were obtained using a Hitachi S5500 high-resolution scanning electron microscope (SEM) (Japan) equipped with a Thermo Scientific Instrument accessory for energy dispersive X-ray spectral analysis (United States). For the EDS analysis, the depth of penetration of the scanning beam was ~1 μm.

This set does not allow determining the composition of the samples that are easily magnetized. Therefore, the data on the surface morphology and element composition of the fibers from FeCrAl alloy were obtained using a JXA 8100 X-ray spectral microanalyzer (Japan) additionally equipped with an INCA energy-dispersive accessory (Great Britain). In this case (for X-ray microprobe analysis), the depth of penetration of the scanning beam was ~2–5 μm.

The fiber diameter ($d$) was measured using a micrometer: the average value was calculated from 5–15 measurements. The specific geometric surface ($S_{spec\ geom}$) was calculated according to the formula $S_{spec\ geom} = 4/\rho \cdot d$, where ρ is the alloy density, assuming that the area of fiber butt ends is infinitely smaller than that of their side area.

### 2.4. Catalytic tests of fibrous samples

The catalytic activity of fiber samples in the reaction of oxidation of CO into $CO_2$ was determined from the dependence of the CO conversion on temperature. Samples of metallic fibers for catalytic tests were selected in such a way as to make their geometric surface area equal to about 50 $cm^2$. The prepared samples (Fig. 3, upper row) were placed into the reaction zone of a tubular quartz reactor between quartz sand layers. The catalytic-test conditions: a BI-CATflow 4.2(A) flow-type catalytic system (Institute of Catalysis, Siberian Branch, Russian Academy of Sciences, Russia); gas-mixture composition 5% CO + air; and rate of gas flow through the reactor (volume 3 $cm^3$) 50 mL/min. At each temperature, a sample was preliminarily held for 20 min to ensure homogeneous bulk temperature distribution, after which CO and $CO_2$ concentrations were measured at the reactor inlet and outlet using a PEM–2 gas analyzer (Institute of Catalysis, Russia).

## 3. Results

### 3.1. Initial fibers

The metallic fibers diameters, alloy densities, and calculated specific geometric surfaces are shown in Table 1. Their appearances are shown in Fig. 3, and the images obtained with the help of scanning electron microscopy (SEM) – in Fig. 4. The fibers appear to be inhomogeneous in thickness and contain defects on their surfaces (Fig. 4). Comparison of the data of XRF (analysis depth is up to 20 μm) and energy-dispersive X-ray spectral analysis (depth of analysis is 2–5 μm for FeCrAl alloy and 1 μm for other fibers) shows that the fiber surface is covered with an oxide film and contaminated with carbon. Only in the case of FeCrAl alloy, carbon and oxygen are not found on the surface.

As can be seen from the results of catalytic tests of fiber samples in the oxidation of CO into $CO_2$ (Fig. 5a), the CO conversion values at 500 °C are equal to 12, 5, and 4% on fibers made of FeCrAl alloy, aluminum alloy, and technical grade titanium, respectively. The latter means that these samples are inactive in CO oxidation in the investigated temperature range. Copper fibers are active in CO oxidation at temperatures above 200 °C. At 300 °C, the degree of CO conversion on Cu fibers attains 100%. However, in the second cycle of catalytic tests, the graph of the dependence $X = f(T)$ shifts to higher temperatures, which indicates a partial deactivation of Cu fibers.

After catalytic tests, aluminum fibers become slightly yellowish, titanium ones turn into blue-violet, fibers made of FeCrAl alloy become brown, and golden-pink copper fibers turn black (Fig. 3), which indicates the formation of oxides on their surface. The change in the color of fibers is accompanied by the change in the morphology of the surface, as can be seen on the example of copper fibers (Fig. 6). The surface of the initial copper fibers contains defects in the

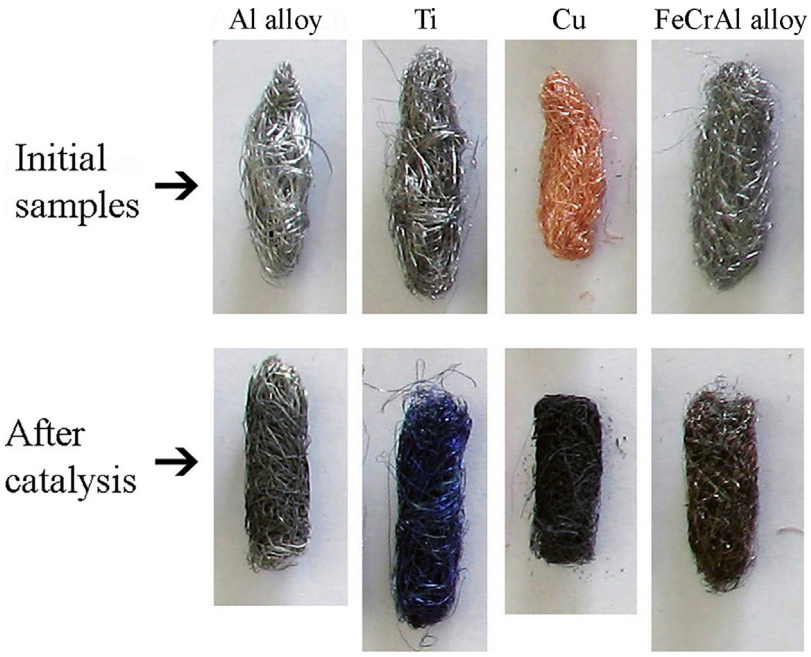


**Fig. 3.** Photographs of initial metal fibers prepared for catalytic tests and those after catalytic tests.

**Table 1**
Characteristics of metallic fibers: average diameter *d* and length *l*, alloy density ρ, calculated specific geometric surface area $S_{spec.\ geom}$, and element composition according to XRF (analysis depth is 10–20 μm) and EDS (analysis depth is ~1 μm).

| System | Element composition, wt. % | | *l*, cm | *d*, mm | $\rho$, g/cm$^3$ | $S_{spec\ geom.}$, cm$^2$/g |
|---|---|---|---|---|---|---|
| | XRF | EDS | | | | |
| Al-Mg-Cu (1160 aluminum alloy) | 89.1 Al, 2.1 Mg, 3.4 Cu, 0.51 Mn, 0.25 Fe, 0.19 Zr, 0.05 Si, 0.01 Cr, 0.09 Zn, 0.08 Ti | 64.2 Al, 0.9 Mg, 2.4 Cu, 27.1 C, 5.4 O, 0.03 Si | 10-20 | 0.10 ± 0.01 | 2.80 | 138 |
| Ti (VT1-0) | 99.0–99.7 Ti, 0.2–0.9 Al, 0.07 Fe, Impurities: 0.01 Mo, 0.01 V, 0.07 Cr, 0.04 Cu, 0.06 Sn | 92.4 Ti, 0.1 Al, 6.0 C, 1.5 O | 10-30 | 0.07 ± 0.01 | 4.505 | 125 |
| Cu (M2) | 99.3–99.8 Cu, 0.05–0.11 Ni, Impurities: 0.12–0.15 Zn, 0.01 Mn, 0.57 Si, 0.06 Zr | 86.0 Cu, 11.0 C, 3.0 O | ~0.5 | 0.068 ± 0.006 | 8.94 | 66 |
| FeCrAl alloy (Cr23Al5 heat-resistant steel) | 73.2Fe, 22.8 Cr, 3.6 Al, 0.4 Ti | (*) 71.3 Fe, 24.8 Cr, 4.4 Al, 0.4 Ti | 5-20 | 0.052 ± 0.005 | 7.25 | 106 |

*Note:* (*) Data of X-ray microprobe analysis, depth of analysis is 2–5 μm.

**Table 2**
Element composition (at.%) of copper fibers and copper-coated fibers before and after catalytic tests according EDS (*) and X-ray microprobe analysis (**).

| System | Initial surface (before catalysis) | | Surface after catalysis | |
|---|---|---|---|---|
| | Copper-coated fiber site | Uncoated fiber site | Copper-coated fiber site | Uncoated fiber site |
| Cu* | 39.4–70.0 (56.9) Cu<br>0–13.0 (6.8) O<br>28.4–47.5 (36.4) C | | 20.2–39.2 (30.1) Cu<br>25.9–36.5 (32.2) O<br>27.8–44.3 (37.6) C | |
| Cu/Al-alloy* | 39.0–66.0 (55.4) Cu<br>0.4–3.4 (1.3) Al<br>11.0–18.0 (13.4) O<br>18.6–49.4 (29.7) C | 1.9–22.2 (7.3) Cu<br>28.2–98.1 (63.3) Al<br>0–2.4 (0.8) Mg<br>0–49.5 (13.8) O<br>0–42.9 (14.8) C | 4.4–40.4 (17.0) Cu<br>0.7–3.6 (2.8) Al<br>16.4–46.1 (26.8) O<br>12.8–68.5 (53.4) C | 0–6.2 (2.9) Cu<br>19.6–58.5 (58.6) Al<br>0–2.0 (1.1) Mg<br>5.0–15.8 (8.9) O<br>0–64.6 (28.6) C |
| Cu/Ti* | 56.8–73.7 (65.1) Cu<br>0–0.4 (0.1) Ti<br>0–12.6 (7.2) O<br>25.3–30.6 (27.6) C | 0.5–5.2 (2.8) Cu<br>91.8–99.5 (95.9) Ti<br>0 O<br>0–11.2 (5.0) C | 30.3–34.8 (31.7) Cu<br>–<br>37.4–42.2 (40.1) O<br>23.1–30.7 (28.2) C | 0.4–3.1 (1.3) Cu<br>12.1–96.6 (70.0) Ti<br>0–35.6 (12.4) O<br>2.7–33.2 (12.5) C<br>0–31.6 (4.3) N |
| Cu/FeCrAl alloy** | 77.9–80.1 (78.8) Cu<br>0.9–2.7 (1.9) Fe<br>0.3–1.0 (0.6) Cr<br>0 Al<br>0–9.9 (6.0) O<br>9.6–16.2 (12.7) C | 0.3–0.5 Cu<br>60.4–68.2 Fe<br>22.1–24.5 Cr<br>6.3–9.3 Al<br>0 O<br>0–7.5 C | 50.1–60.1 (55.9) Cu<br>0.4–1.8 (0.9) Fe<br>0–0.5 (0.2) Cr<br>0 Al<br>30.4–42.1 (35.0) O<br>5.5–11.1 (8.0) C | 0.4 Cu<br>61.8 Fe<br>22.3 Cr<br>9.2 Al<br>0 O<br>5.5 C |

*Note:* The average concentration of the element is indicated in parentheses.

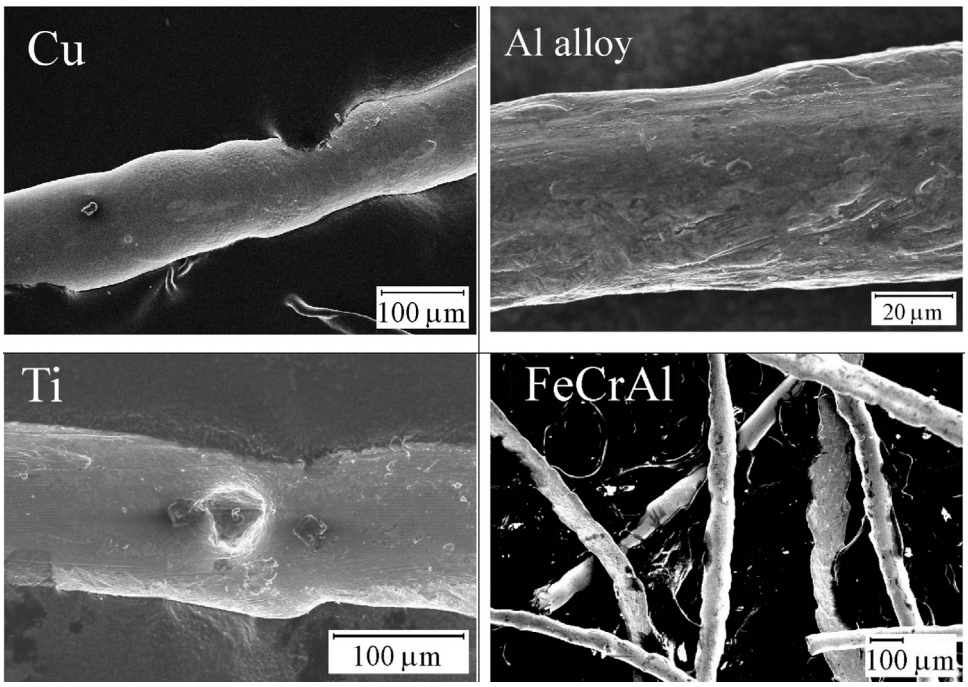


**Fig. 4.** SEM images of the surface of the initial fibers.

form of granules and irregularities (Fig. 6a). Upon the interaction with the reaction mixture (CO, $CO_2$, and air) at elevated temperatures, the surface becomes covered with nanosized structures in the form of "flakes" (Fig. 6b). According to the EDS data, the amount of oxygen on the surface layer of copper fibers increases after catalysis, thereby decreasing the copper concentration (Table 2, Fig. 7). The atomic ratio of O:Cu ≈ 1:1 corresponds to the CuO formation.

### 3.2. Copper-coated fibers: the composition, surface morphology, and catalytic activity

As a result of electroless copper plating and copper electroplating, the fibers made of aluminum alloy, titanium, and FeCrAl alloy acquire a golden-pink color (Fig. 2d) like that of copper fibers. According to visual observations and analysis of SEM images, it can be concluded that the copper coatings deposited under the selected conditions did not completely cover the surface of the fibers. The formed copper coatings look like rows of globules located along aluminum and titanium fibers (Fig. 8bce). The formed copper coatings of globules are arranged along the aluminum and titanium fibers (Fig. 8bce). The diameters of such globules are 2-3 and 10-20 μm for aluminum and titanium fibers, respectively, and coincide with the thicknesses of the corresponding copper coatings. The surface of copper globules is uneven and bumpy (Fig. 8cf). On the sites unclosed with copper layers, convex light strips are visible on the surface of aluminum fibers (Fig. 8b).

In addition to copper, the elements of metal substrates, such as aluminum, titanium, iron, and chromium, are found in the composition of copper coatings (Table 2, Fig. 7). In the composition of copper-uncoated sites, the concentrations of these elements are higher. Oxygen is detected on the surfaces of all copper coatings. However, oxygen is not found on the surface of copper-uncoated sites of the fibers from titanium and FeCrAl alloy, while its concentration is higher in similar sites of aluminum alloy fibers.

The deposition of copper coatings on metal fibers made of aluminum alloy, titanium, and FeCrAl alloy leads to an increase in their activity in CO oxidation (Fig. 5bcd) as compared to the initial ones (Fig. 5a). For Cu/Ti and Cu/Al, the graphs of the temperature dependence of CO conversion are shifted to higher temperatures in the second cycle of catalytic tests; later, the conversion values are stabilized. For Cu/FeCrAl, the course of the curve $X = f(T)$ remains virtually unchanged. According to the catalytic activity (in decreasing order) based on the temperature of 50% conversion of CO ($T_{50}$), the copper-coated fibers can be ranged in the series: Cu ≈ Cu/FeCrAl > Cu/Al > Cu/Ti (Fig. 5e). Thus, the activity of copper-coated fibers from the FeCrAl alloy in CO oxidation is comparable to that of copper fibers.

### 3.3. Change in surface morphology and composition of copper-coated fibers during catalytic tests

Catalytic tests result in changes in the appearance and color of the copper-coated fibers. The copper-coated sites become black, uncoated sited of the fibers from aluminum alloy and FeCrAl alloy acquire a yellowish tint, whereas similar sites of titanium fibers become blue-violet.

In SEM images (Fig. 9adg) of the surface of the copper-coated fibers after catalysis, two types of sites can be distinguished: coarse rough protruding and smooth ones. The surface structure of the rough flake-like sites on aluminum alloy and titanium fibers (Fig. 9be) is similar to those of copper fibers after catalysis (Fig. 6b). In all cases, the flake sizes are virtually the same – 300–700 nm. At higher magnification, one can see that smooth sites have different structures. However, there are separated dispersed particles (Fig. 9c) or their placers (Fig. 9f) on the fiber surfaces of titanium and aluminum alloy. The sizes of dispersed particles are 50–100 nm for aluminum alloy fibers and 100–200 nm for titanium fibers.

Flake-like sites consist mainly of copper, oxygen, and carbon (Table 2, Fig. 7). For these sites, the O:Cu atomic ratio is about 1 in case of copper fibers (1.07), >1 for Cu/Al (1.57) and Cu/Ti (1.26), and <1 (0.63) for Cu/FeCrAl.

The smooth sites contain mainly fiber elements and small quantities of copper and oxygen (Table 2, Fig. 10). In the case of fibers made of the FeCrAl alloy, oxygen is completely absent. This means that copper-uncoated sites on the surface of aluminum and tita-

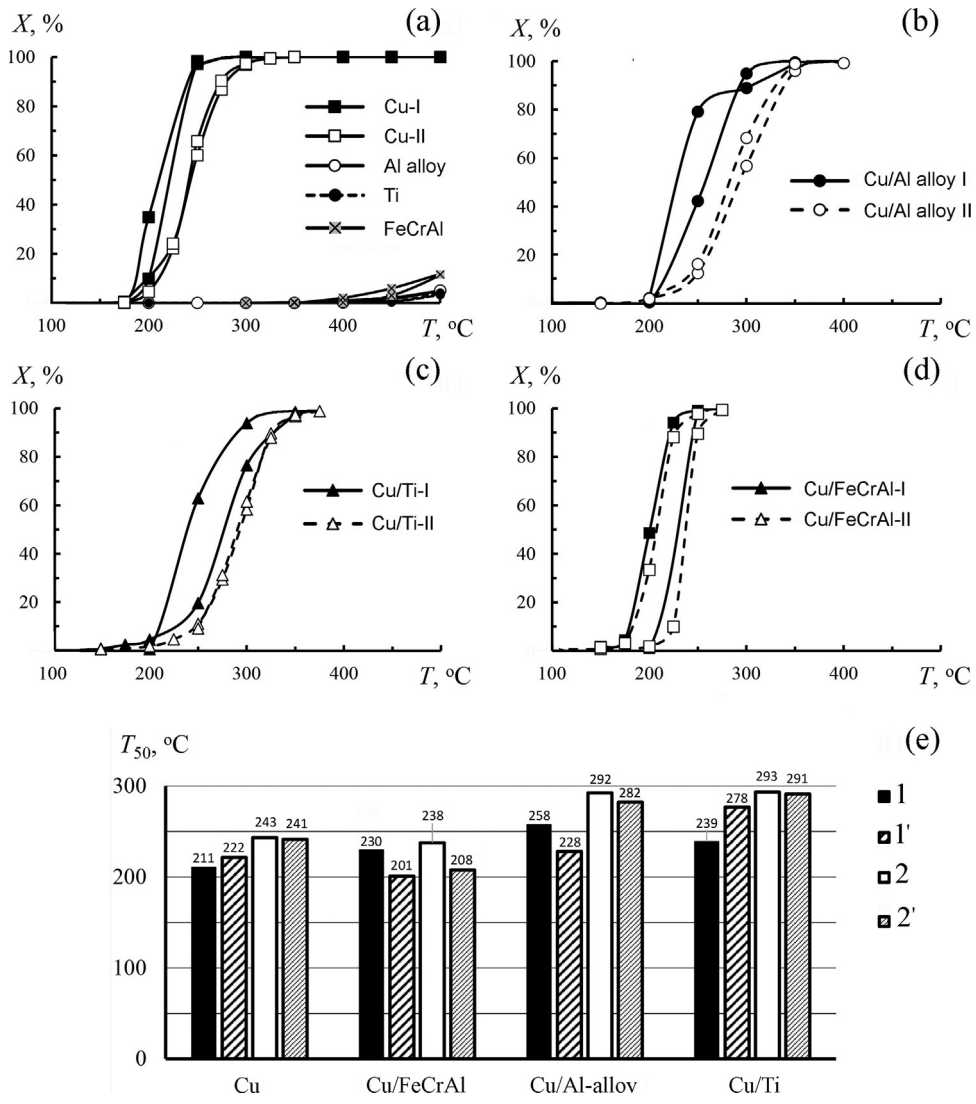


**Fig. 5.** Conversion vs. temperature: (a) for initial metal fibers and (bc) for copper-coated fibers from aluminum alloy (b), titanium (c), FeCrAl alloy (d) in the first (I) and second (II) cycles of catalytic tests. The temperatures of 50% conversion (e) for copper and copper-coated fibers in the first (1, 1′) and second (2, 2′) cycles of catalytic tests at heating (1, 2) and cooling (1′, 2′).

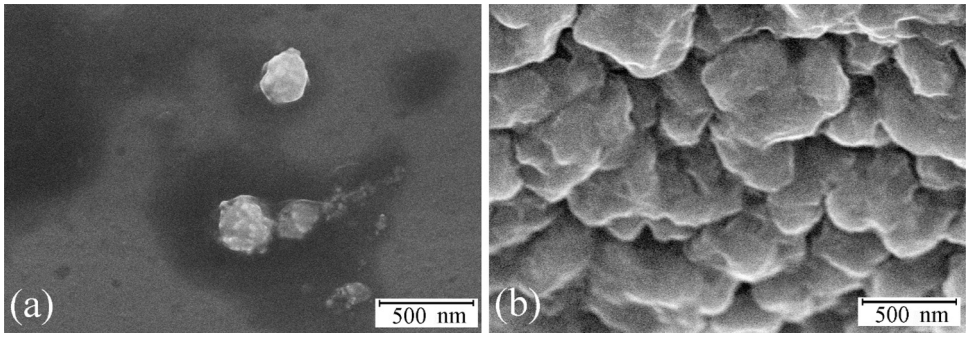


**Fig. 6.** SEM images of the surface of copper fibers before and after catalytic tests.

nium fibers are partially oxidized, while the fibers made of FeCrAl alloy does not undergo oxidation under the experimental conditions. Copper is concentrated in dispersed particles on the surface. For example, light sites with placers of dispersed particles in Fig. 9f contain 1.2–1.9 at.% Cu, while neighboring darker areas do only about 0.4 at.% Cu.

## 4. Discussion

All the copper-coated fibers under study are active in deep CO oxidation. The temperature range of their activity in this reaction is similar to that of copper fibers, all of them convert CO into $CO_2$ at a temperature above 200 °C. As follows from the obtained results

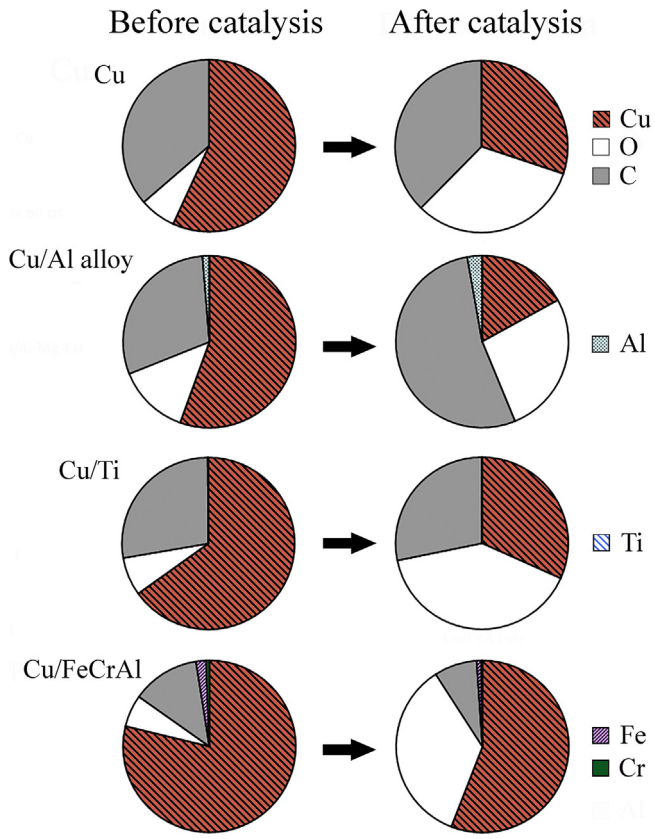


**Fig. 7.** Composition of copper fibers and copper-coated sites of the fibers from aluminum alloy of the system Al-Mg-Cu, titanium and FeCrAl alloy before and after the catalytic tests.

and their comparison with the available literature data, the copper oxide formation on both copper fibers and copper-coated sites on titanium, aluminum, or FeCrAl alloy during catalytic tests determine the catalytic activity of the samples. According to the decrease in the catalytic activity, the investigated samples are arranged in the series Cu ≈ Cu/FeCrAl > Cu/Al > Cu/Ti (Fig. 5e). The activity of copper-coated fibers made of FeCrAl alloy is comparable to the activity of copper fibers. The deposition of copper coatings on fibers made of FeCrAl alloy, on the one hand, will reduce the consumption of copper and the mass of products, and, on the other hand, allows increasing the temperature range of their use due to higher heat resistance of the carrier.

The increased catalytic activity in the case of Cu/FeCrAl fibers is correlated to higher copper content in the composition of the copper-coated sites (Table 2). However, the differences in the copper content can be associated with different methods of analysis in the case of Cu/FeCrAl and in other samples. To study the composition of coatings for Cu/FeCrAl, the X-ray microprobe analysis was used due to the ferromagnetic properties of the FeCrAl-alloy, while the EDS method was used for other samples. However, it is possible that the main reason for the difference in the copper content consists in surface contamination by carbon, which is much lower in the case of Cu/FeCrAl. Since the outer layer is usually carbonized, and the depth of analysis is different, the lower is the carbon contamination and the greater is the analysis depth, the less carbon is found in the analyzed layer. If we subtract the carbon content and recalculate the data in Table 2, the copper concentration in the coatings will be (at.%): 89.3 (Cu), 79.0 (Cu/Al), 89.9 (Cu/Ti), and 90.3 (Cu/FeCrAl). That is, the spread of copper concentrations is not so significant.

Unlike copper fibers, copper on the surface of fibers made from titanium, aluminum, or FeCrAl alloy does not form continuous layers. According to Fig. 8adg, the isolated islands of copper occupy not less than 50% of the surface of metal fibers. Some decrease in the activity of CO oxidation for the copper-coated fibers made of alu-

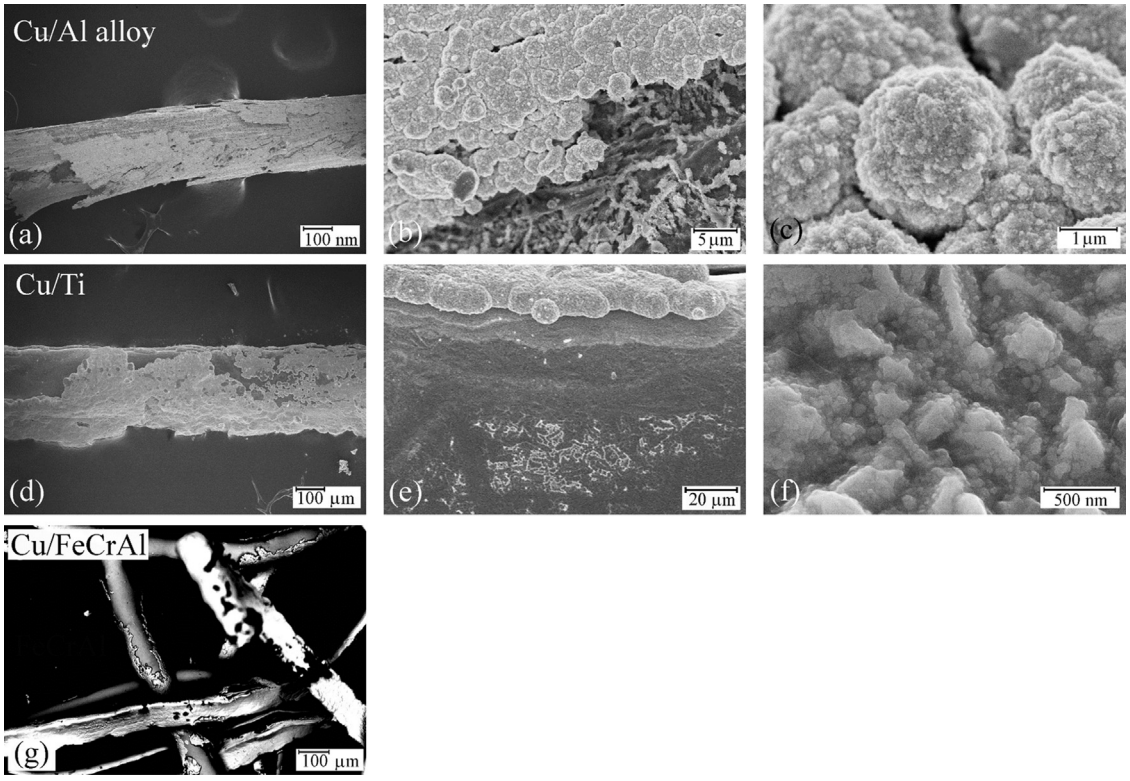


**Fig. 8.** SEM images of copper-coated fibers from aluminum alloy of the system Al-Mg-Cu (a–c), titanium (d–f) and FeCrAl alloy (g).

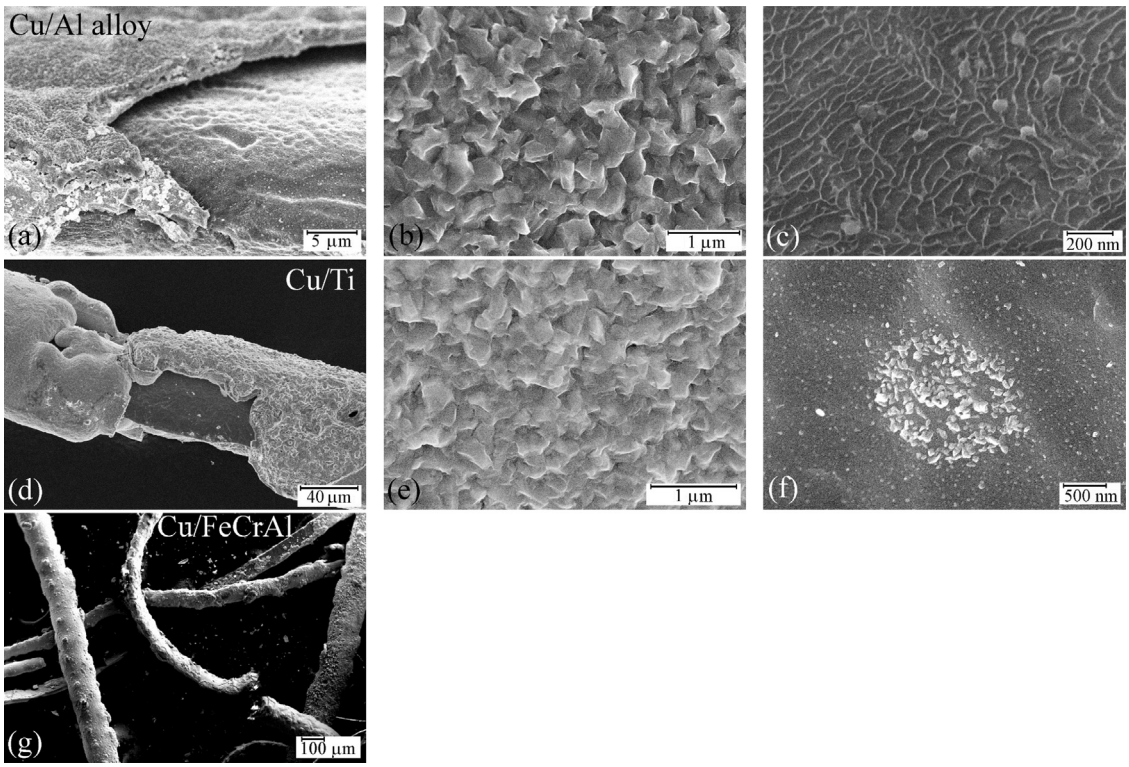


**Fig. 9.** SEM images of copper-coated fibers from aluminum alloy of the system Al-Mg-Cu (a–c), titanium (d–f) and FeCrAl alloy (g) after the catalytic tests.

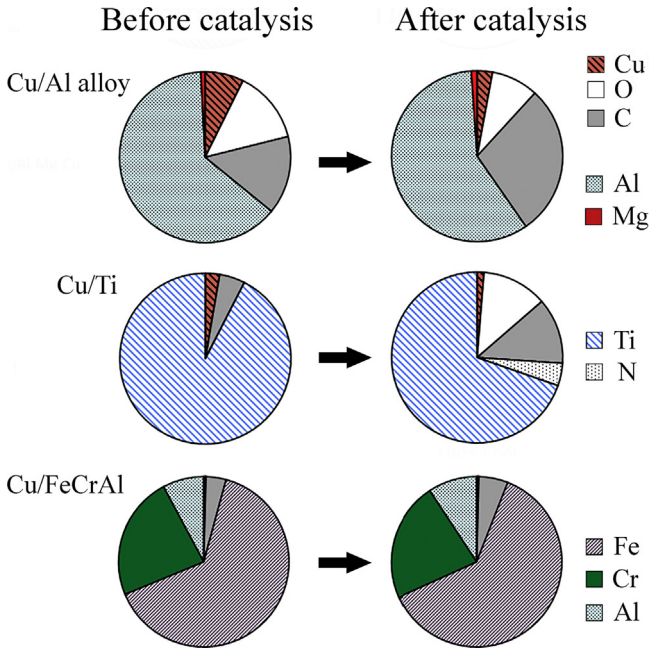


**Fig. 10.** Composition of copper-uncoated sites of the metal fibers before and after the catalytic tests.

minum alloy and titanium can be related to both the smaller area occupied by the active compound on the surface and the effect of the fiber material and oxides from this material. The comparable activity of copper fibers and copper-coated samples of FeCrAl alloy in CO oxidation indicates the determining effect of the second factor. In this case, the area of copper-coated sites is comparable with that of aluminum alloy and titanium, but no oxidation of the fiber material on uncoated sites was detected (Fig. 10).

The higher activity of Cu/FeCrAl in comparison with Cu/Al and Cu/Ti is, probably, the result of the substrate effect. Since, first, the FeCrAl-alloy substrate itself has a slightly higher activity, in comparison with aluminum and titanium (Fig. 5a), Cu-uncoated sites of Cu/FeCrAl must be more active than those of Cu/Al and Cu/Ti.

Second, it cannot be ruled out that on the copper-free surface of the Cu/FeCrAl fibers the sites with chromium and iron oxides are formed as a result of interaction with oxygen. Chromium and iron oxides formed under elevated temperatures are more active than titania and alumina [45]. In accordance with the relative activity in CO oxidation at 300 °C (1% CO in $O_2$ excess) [23], the base metal oxide catalysts can be ranged as: $CuO(45) > Fe_2O_3(0.4) > Cr_2O_3(0.03)$. The similar series of activity is confirmed for reaction mixtures with a stoichiometric components ratio under stationary conditions at 500 °C [45]. Using the X-ray microprobe analysis method, we did not find oxygen on the copper-free surface of Cu/FeCrAl fibers (Fig. 10). However, according to [46], a thin native oxide of a thickness of 2–3 nm covers the surface of FeCrAl alloy. This oxide contains Fe, Cr and, Al, where Fe and Cr enrich the outer and inner parts of the oxide, respectively. Since the concentration of iron on the surface of the oxide film is higher than that of chromium, it can have a greater effect on the catalytic activity of Cu/FeCrAl samples.

Third, at elevated temperatures, interaction between copper species (Cu, $Cu_2O$, CuO) and fiber underlayers containing Fe, Cr, and Al is possible with the formation of spinels. The catalytic activity of $CuCr_2O_4$ and $CuFe_2O_4$ in CO oxidation is higher than that of $CuAl_2O_4$ [21,23,47–50]. This can be one of the reasons for the increased activity of Cu/FeCrAl fibers.

As the duration of the catalytic tests increases, the activity of copper fibers and copper-coated ones decreases. There are two reasons for the decrease in the catalytic activity of copper and copper-coated fibers. The first consists in sintering of copper particles on the fibers surface at elevated temperatures, which reduces the catalytically active phase area. The second reason is an increase

in the fraction of CuO. Upon contact with a reaction gas mixture containing both the oxidizing agent ($O_2$) and the reducing agent (CO), all three types of copper species (Cu°, $Cu_2O$ and CuO) can simultaneously coexist on the surface of copper and copper-coated fibers. According to the data of [20,51], $Cu_2O$ is the most active among copper species. As the temperature increases, the fraction of CuO increases [20].

Regardless of the methods used (electroless copper plating for aluminum alloy or copper electroplating for titanium), copper forms spherical objects (globules) on the fiber surfaces. These globules eventually merge over time to form copper-coated sites or islands (Fig. 8bce). The globule sizes are different for the fibers from aluminum alloy and titanium. Unfortunately, we could not study the structural features of such formations and estimate their sizes for the fibers from FeCrAl alloy, since Hitachi S5500 high-resolution scanning microscope does not allow studying magnetizable samples. Therefore, at this stage of research, it is difficult to separate the effect of the nature of metal fiber and the method of copper deposition on the sizes of copper-containing spherical formations.

After catalytic tests, the surface structure of copper-coated sites (Fig. 9bd) on the fibers made of aluminum alloy and titanium is similar to that of copper fibers (Fig. 6b). In all cases, the surface is coated with flakes, the sizes of which are 300–700 nm. According to the element composition data (Table 2 and Fig. 7), copper oxide predominates in the flake composition.

After catalysis, the atomic oxygen-to-copper ratio is 1 for copper fibers (1.07), >1 for Cu/Al (1.57) and Cu/Ti (1.26), and <1 (0.63) for Cu/FeCrAl fibers. If we take into account only the ratio of oxygen to copper (without consideration of carbon and impurity atoms), in the first case, this Cu/O ratio is an evidence for the formation of CuO, in the second and the third ones, it indicates the presence, together with CuO, of adsorbed oxygen compounds on the surface, for example, such as water, hydroxyl, or carbonate groups. The ratio $0.5 < Cu/O < 1$ indicates to the formation of CuO and $Cu_2O$. On the one hand, the presence of $Cu_2O$ in the composition of the surface layer of Cu/FeCrAl fibers could be another reason for its higher activity compared to activities of Cu/Al and Cu/Ti. On the other hand, it can not be excluded that, in the case Cu/FeCrAl, the surface layer after catalysis consists mainly of CuO, and the copper excess in comparison with oxygen is due to the fact that underlying layers of the copper coating affect the result of analysis.

As was mentioned in the Introduction, depending on the temperature treatment of copper in oxygen-containing media, copper oxides in the form of nanosized rods, sheets, flowers, etc. can be fabricated on its surface, which increases the specific surface area and the activity of copper catalysts [34–37,41,43]. For example, in [36], copper oxide nanowhiskers were observed as a result of air annealing the copper coatings deposited on stainless steel mesh for 4 h at temperatures of 200–500 °C. In our case, nanosized flakes are formed. Consequently, different heat treatment conditions and different composition of the gas atmosphere lead to different morphological formations on the surface of the copper coating.

The catalytic activity is related to the composition of the surface layer. Fig. 7 shows the composition of copper layers before and after catalytic tests. In the composition of copper coatings on fibers from FeCrAl alloy, the concentration of copper is even higher than in the composition of the copper fibers themselves, since the latter are contaminated with carbon. Contamination of fibers by carbon can be caused by both fabrication method features and subsequent manipulation with the samples and basic carbonate formation on the copper surface by contact with moist air containing carbon dioxide: $2Cu + O_2 + CO_2 + H_2O \rightarrow Cu(OH)_2 \cdot CuCO_3$ [52]. At the same time, it is possible that high concentration of copper and lower concentration of carbon in the copper coatings on the fibers from FeCrAl alloy are associated with a greater depth of analysis in this case (Section 2.3).

## 5. Conclusions

Metal fibers formed by the pendant drop melt extraction (PDME) method are promising for the use in the design of catalysts from the point of their composition, surface structure, and size. However, for their application in this capacity, it is necessary to justify the methods of modifying their surface with catalytically active components. The results of the present work show that electrolplating and electroless plating copper onto fiber surfaces can serve as such methods of modification. It is also possible to deposit other transition or noble metals onto the surface of the fibers, conduct subsequent annealing, and realize other types of additional processing.

## Acknowledgments

The work was carried out within the Institute of Chemistry FEBRAS State Order (project no. 265-2014-0001) and partially supported by grants of and the FEBRAS Program “Far East” (project no. 265-20-15-0022).

## References

[1] S.F. Tikhov, G.V. Chernykh, V.A. Sadykov, A.N. Salanov, G.M. Alikina, S.V. Tsybulya, V.F. Lysov, Honeycomb catalysts for clean-up of diesel exhausts based upon the anodic-spark oxidized aluminium foil, Catal. Today 53 (4) (1999) 639–646.
[2] P. Avila, M. Montes, E.E. Miro, Monolithic reactors for environmental applications - A review on preparation technologies, Chem. Eng. J. 109 (13) (2005) 11–36.
[3] V.S. Beskov, E.A. Brushtein, E.V. Golovnia, V.I. Vanchurin, Modeling of ammonia oxidation on platinoid grids, Catal. Ind. (2) (2008) 31–36 (in Russian) https://elibrary.ru/download/elibrary_11674260_44102609.pdf.
[4] M.M. Zyryanova, P.V. Snytnikov, Y.I. Amosov, V.A. Kuzmin, V.A. Kirillov, V.A. Sobyanin, Design, scale-out, and operation of a preferential CO methanation reactor with a nickel-ceria catalyst, Chem. Eng. J. 176 (SI) (2011) 106–113.
[5] H. Kierzkowska-Pawlak, P. Tracz, W. Redzynia, J. Tyczkowski, Plasma deposited novel nanocatalysts for $CO_2$ hydrogenation to methane, J. $CO_2$ Util. 17 (2017) 312–319.
[6] C. Neagoe, D.C. Boffito, Z.N. Ma, C. Trevisanut, G.S. Patience, Pt on Fecralloy catalyses methane partial oxidation to syngas at high pressure, Catal. Today 270 (2016) 43–50.
[7] A. Kolodziej, J. Lojewska, J. Tyczkowski, P. Jodlowski, W. Redzynia, M. Iwaniszyn, S. Zapotoczny, P. Kustrowski, Coupled engineering and chemical approach to the design of a catalytic structured reactor for combustion of VOCs: cobalt oxide catalyst on knitted wire gauzes, Chem. Eng. J. 2000 (2012) 329–337.
[8] RF Patent 2215579 (2003).
[9] M.S. Pasechnik, Development of a Metal-Fiber Catalyst Based on Nickel and the Technology of Its Production by the Method of High-Speed Solidification of the Melt (Ph. D. Thesis) (In Russian), MATI – K. E. Tsiolkovsky Russ. State Technol. Univ., Moscow, 2003 http://www.dissercat.com/content/razrabotka-metallovoloknistogo-katalizatora-na-osnove-nikelya-i-tekhnologii-ego-polucheniya-.
[10] J.V. Wood, P.F. Mills, A.R. Waugh, J.V. Bee, Rapidly solidified nickel-base super-alloys, J. Mater. Sci. 15 (11) (1980) 2709–2719.
[11] V.A. Vasiliev, B.S. Mitin, I.N. Pashkov, M.M. Serov, A.A. Skuridin, A.A. Lukin, V.B. Yakovlev, in: B.S. Mitin (Ed.), High-Speed Solidification of Melts (Theory, Technology, Materials), SP Intermet Engineering, Moscow, 1998 (in Russian).
[12] B.V. Borisov, M.M. Serov, Forming porous fibrous materials by the pendant drop melt extraction, Rus. J. Non-Ferrous Met. 54 (5) (2013) 407–411.
[13] V. Antsyferov, M. Serov, Manufacturing of a Rapid Solidification Materials and Fibers, LAP Lambert Academic Publishing, 2014.
[14] Yu.M. Volfkovich, A.N. Filippov, V.S. Bagotsky, Structural properties of porous materials and powders used in different fields of science and technology, in: Eng. Mater. Process, Springer-Verlag London Ltd., 2014.
[15] H.F. Zhang, A.M. Wang, H. Li, Q.H. Song, B.Z. Ding, Z.Q. Hu, Microstructure and catalytic properties of rapidly quenched Ni-Al-Cr-Fe alloy, Mater. Lett. 48 (6) (2001) 347–350.
[16] M. Pisarek, M. Lukaszewski, P. Winiarek, P. Kedzierzawski, M. Janik-Czachor, Catalytic activity of Cr- or Co-modified Ni-based rapidly quenched alloys in the hydrogenation of isophorone, Appl. Catal. A: Gen. 358 (2) (2009) 240–248.
[17] B. Sun, J. Lin, K. Xu, Y. Pei, S. Yan, M.H. Qiao, X.X. Zhang, B.N. Zong, Fischer–Tropsch synthesis over skeletal FeCe catalysts leached from rapidly quenched ternary FeCeAl alloys, ChemCatChem (5) (2013) 3857–3865.
[18] J.G. Fan, B.N. Zong, X.X. Zhang, X.K. Meng, X.H. Mu, G.B. Yu, M.H. Qiao, K.N. Fan, Rapidly quenched skeletal Fe-based catalysts for Fischer-Tropsch synthesis, Ind. Eng. Chem. Res. 47 (16) (2008) 5918–5923.
[19] V.S. Rudnev, I.V. Lukiyanchuk, M.M. Serov, B.L. Krit, G.D. Lukiyanchuk, D.P. Farafonov, Catalytic properties of metallic fibers fabricated by tempering of

melt on a rotating heat-receiver, Prot. Met. Phys. Chem. Surf. 53 (2) (2017) 287–293.
[20] T.J. Huang, D.H. Tsai, CO oxidation behavior of copper and copper oxides, Catal. Lett. 87 (3-4) (2003) 173–178.
[21] R. Prasad, P. Singh, A review on CO oxidation over copper chromite catalyst, Catal. Rev.-Sci. Eng. 54 (2) (2012) 224–279.
[22] E.A. Trusova, M.V. Tsodikov, E.V. Slivinskii, G.G. Hernandez, O.V. Bukhtenko, T.N. Zhdanova, D.I. Kochubei, J.A. Navio, The effect of the structure of Cu-Ti oxide systems obtained by sol-gel synthesis on the nature of catalytic centres and catalytic activity in low-temperature CO oxidation, Mendeleev Commun. (3) (1998) 102–104 http://pubs.rsc.org/-/content/articlepdf/1998/mc/a800893k.
[23] S. Royer, D. Duprez, Catalytic oxidation of carbon monoxide over transition metal oxides, ChemCatChem 3 (2011) 24–65.
[24] Yu. N. Naguriankaya, E.A. Vlasov, Creation of catalytically active oxide layers on surfaces of copper and brass, Bull. St PbIT (TU) (32) (2015) 17–23, http://dx.doi.org/10.15217/issn998984-9.2015.32.17 [In Russian].
[25] G. Xanthopoulou, G. Vekinis, Investigation of catalytic oxidation of carbon monoxide over a Cu–Cr-oxide catalyst made by self-propagating high-temperature synthesis, Appl. Catal. B: Environ. 19 (1) (1998) 37–44.
[26] L.C. Loc, H.T. Cuong, N. Tri, H.S. Thoang, A study on the properties of modified CuO samples and the kinetics of carbon monoxide oxidation over the given catalysts, J. Exp. Nanosci. 6 (6) (2011) 631–640.
[27] A.N. Pestryakov, A.A. Fyodorov, M.S. Gaisinovich, V.P. Shurov, I.V. Fyodorova, T.A. Gubaydulina, Metal-foam catalysts with supported active phase for deep oxidation of hydrocarbons, React. Kinet. Catal. Lett. 54 (1) (1995) 167–172.
[28] Z. Boukha, J.L. Ayastuy, A. Iglesias-Gonzalez, B. Pereda-Ayo, M.A. Gutierrez-Ortiz, J.R. Gonzalez, Velasco, New copper species generated on $Cu/Al_2O_3$-based microreactors for COPROX activity enhancement, Int. J. Hydrogen Energy 40 (23) (2015) 7318–7328.
[29] J.A. Rodriguez, P. Liu, X. Wang, W. Wen, J. Hanson, J. Hrbek, M. Peŕez, J. Evans, Water-gas shift activity of Cu surfaces and Cu nanoparticles supported on metal oxides, Catal. Today 143 (2009) 45–50.
[30] D.-W. Jeong, W.-J. Jang, J.-O. Shim, W.-B. Han, H.-S. Roh, U.H. Jung, W.L. Yoon, Low-temperature water-gas shift reaction over supported Cu catalysts, Renew. Energy 65 (2014) 102–107.
[31] S. Bennici, A. Gervasini, Catalytic activity of dispersed CuO phases towards nitrogen oxides ($N_2O$, NO, and $NO_2$), Appl. Catal. B: Environ. 62 (34) (2006) 336–344.
[32] P. Carniti, A. Gervasini, V.H. Modica, N. Ravasio, Catalytic selective reduction of NO with ethylene over a series of copper catalysts on amorphous silicas, Appl. Catal. B: Environ. 28 (3-4) (2000) 175–185.
[33] Y.-K. Lin, Y.-H. Su, Y.-H. Huang, C.-J. Hsu, Y.-K. Hsu, Y.-G. Lin, K.-H. Huang, S.-Y. Chen, K.-H. Chen, L.-C. Chen, Efficient hydrogen production using Cu-based catalysts prepared via homogeneous precipitation, J. Mater. Chem. 19 (2009) 9186–9194.
[34] M.M. Momeni, M. Mirhosseini, Z. Nazari, A. Kazempour, M. Hakimiyan, Antibacterial and photocatalytic activity of CuO nanostructure films with different morphology, J. Mater. Sci.—Mater. Electron. 27 (8) (2016) 8131–8137.
[35] Q.F. Fan, Q. Lan, M.L. Zhang, X.M. Fan, Z.W. Zhou, C.L. Zhang, Preparation and photocatalytic activities of 3D flower-like CuO nanostructures, J. Semicond. 37 (8) (2016), 083002, http://dx.doi.org/10.1088/1674–4926/37/8/083002.
[36] A.Y. Kozlov, M.V. Dorogov, N.V. Chirkunova, I.M. Sosnin, A.A. Vikarchuk, A.E. Romanov, CuO nanowhiskers-based photocatalysts for wastewater treatment, Nano Hybrids Compos. 13 (2017) 183–189.
[37] Y. Xi, C.G. Hu, P.X. Gao, R.S. Yang, X.S. He, X. Wang, B.Y. Wan, Morphology and phase selective synthesis of $Cu_xO$ (x = 1, 2) nanostructures and their catalytic degradation activity, Mater. Sci. Eng. B: Adv. Funct. Solid-State Mater. 166 (1) (2010) 113–117.
[38] O.V. Chub, V.V. Mokrinsky, S.I. Reshetnikov, N.A. Yazikov, Yu.V. Dubinin, A.D. Simonov, V.A. Yakovlev, Kinetics of oxidation of carbon monoxide on industrial copper-containing catalyst for fluidized bed, Catal. Ind. 5 (5) (2013) 54–58 [In Russian] http://kalvis.ru/katalog-izdanij/zhurnalyi/kataliz-v-promyishlennosti/arxiv/2013/%E2%84%965/.
[39] L. Lloyd, Handbook of Industrial Catalysts (Fundamental and Applied Catalysis), Springer, 2017.
[40] N.M. Popova, Purification Catalysts for Vehicle Exhaust Gases, Nauka, Almaty, Kazakhstan, (in Russian), 1987.
[41] C.A. Neyertz, A.D. Gallo, M.A. Ulla, J.M. Zamaro, Nanostructured $CuO_x$ coatings onto Cu foils: Surface growth by the combination of gas-phase treatments, Surf. Coat. Technol. 285 (2016) 262–269.
[42] R.L. Papurello, A.P. Cabello, M.A. Ulla, C.A. Neyertz, J.M. Zamaro, Microreactor with copper oxide nanostructured films for catalytic gas phase oxidations, Surf. Coat. Technol. 328 (2017) 231–239.
[43] H. Yan, X.W. Liu, R. Xu, P. Lv, P.H. Zhao, Synthesis, characterization, electrical and catalytic properties of CuO nanowires, Mater. Res. Bull. 48 (6) (2013) 2102–2105.
[44] A.M. Yampolsky, Copper Plating and Nickel Plating, State Scientific and Technical Publishing House of Machine-Building Literature, Moscow, 1961, in Russian http://metallurgu.ru/books/item/f00/s00/z0000013/st007.shtml, or http://metallurgu.ru/books/item/f00/s00/z0000013/index.shtml.
[45] G.K. Boreskov, V.I. Marshneva, Oxidation mechanism of carbon monoxide on 4 period transition metal oxides, Dokl. Akad. Nauk SSSR 213 (1) (1973) 112–115 (in Russian).
[46] P.Y. Hou, X.F. Zhang, R.M. Cannon, Impurity distribution in $Al_2O_3$ formed on an FeCrAl alloy, Scr. Mater. 50 (1) (2004) 45–49, http://dx.doi.org/10.1016/j.scriptamat.2003.09.044.
[47] P.W. Park, J.S. Ledford, Characterization and CO oxidation activity of $Cu/Cr/Al_2O3$ catalysts, Ind. Eng. Chem. Res. 37 (3) (1998) 887–893.
[48] C.C. Chien, W.P. Chuang, T.J. Huang, Effect of heat-treatment conditions on Cu-Cr/ gamma-alumina catalyst for carbon monoxide and propene oxidation, Appl. Catal. A: Gen. 131 (1) (1995) 73–87.
[49] T. Cheng, Z.Y. Fang, Q.X. Hu, K.D. Han, X.Z. Yang, Y.J. Zhang, Low-emperature CO oxidation over $CuO/Fe_2O_3$ catalysts, Catal. Commun. 8 (7) (2007) 1167–1171.
[50] E. Amini, M. Rezaei, M. Sadeghinia, Low temperature CO oxidation over mesoporous $CuFe_2O_4$ nanopowders synthesized by a novel sol-gel method, Chin. J. Catal. 34 (9) (2013) 1762–1767.
[51] V.A. Sadykov, S.F. Tikhov, N.N. Bulgakov, A.P. Gerasev, Catalytic oxidation of CO on CuOx revisited: impact of the surface state on the apparent kinetic parameters, Catal. Today 144 (3-4) (2009) 324–333.
[52] I.L. Knunyants (Ed.), Chemical Encyclopedia, vol. 3, Big Russian Encyclopedia, Moskow, 1992 (in Russian).